Zinc Ions Trigger Conformational Change and Oligomerization of Hepatitis B Virus Capsid Protein[†]

Stephen J. Stray, Pablo Ceres, and Adam Zlotnick*

Department of Biochemistry and Molecular Biology, University of Oklahoma Health Sciences Center, P.O. Box 26901, Oklahoma City, Oklahoma 73190

Received March 2, 2004; Revised Manuscript Received June 1, 2004

ABSTRACT: Assembly of virus particles in infected cells is likely to be a tightly regulated process. Previously, we found that in vitro assembly of hepatitis B virus (HBV) capsid protein is highly dependent on protein and NaCl concentration. Here we show that micromolar concentrations of Zn^{2+} are sufficient to initiate assembly of capsid protein, whereas other mono- and divalent cations elicited assembly only at millimolar concentrations, similar to those required for NaCl-induced assembly. Altered intrinsic protein fluorescence and highly cooperative binding of at least four Zn^{2+} ions ($K_D \sim 7$ μM) indicated that binding induced a conformational change in capsid protein. At 37 °C, Zn^{2+} enhanced the initial rate of assembly and produced normal capsids, but it did not alter the extent of assembly at equilibrium. Assembly mediated by high zinc concentrations ($\geq$300 μM) yielded few capsids but produced a population of oligomers recognized by capsid-specific antibodies, suggesting a kinetically trapped assembly reaction. Comparison of kinetic simulations to in vitro assembly reactions leads us to suggest that kinetic trapping was due to the enhancement of the nucleation rate relative to the elongation rate. Zinc-induced HBV assembly has hallmarks of an allosterically regulated process: ligand binding at one site influences binding at other sites (cooperativity) indicating that binding is associated with conformational change, and binding of ligand alters the biological activity of assembly. We conclude that zinc binding enhances the kinetics of assembly by promoting formation of an intermediate that is readily consumed in the reaction. Free zinc ions may not be the true in vivo activator of assembly, but they provide a model for regulation of assembly.

Hepatitis B virus (HBV) is a small enveloped DNA virus with an icosahedral core. The core is composed of the viral nucleic acid, reverse transcriptase, and the protein capsid (*13*, *15*). In HBV, the capsid is intimately involved in nucleic acid replication in addition to its roles in viral entry and egress. Reverse transcription of the RNA pregenome occurs exclusively within the core particle and produces a gapped double-stranded circular genomic DNA (*36*). The DNA-filled core is then either exported from the cell via the endoplasmic reticulum, where it acquires its envelope, or reimported into the nucleus to maintain infection.

The prevalent form of the core is composed of 120 homodimers of the capsid protein (Cp)[1] arranged with $T = 4$ icosahedral symmetry (*9*, *35*). The structure of the capsid has been determined by cryo-electron microscopy (*4*, *7*, *8*) and X-ray crystallography (*41*), with all structures being in good agreement. In vitro assembled capsids (*46*) and capsids from heterologous expression systems (*4*, *19*, *41*) are morphologically indistinguishable from cores assembled in vivo (M. Yeager et al., personal communication). Capsids are studded with 30 Å long spikes composed of a four-helix bundle, which forms the dimer interface. Antibodies binding the top of the spike (amino acids 70−85) dominate the immune response to intact capsid (HBcAg), based on peptide scanning (*30*) and image reconstruction (*2*, *7*). Murine anti-capsid monoclonal antibodies (mAb) recognize essentially the same epitope as human anti-HBcAg (*30*). In HBV infections, assembled capsid (HBcAg) and an unassembled secreted form of the Cp (HBeAg) elicit distinct antibody responses (*25*, *30*). Unassembled Cp is recognized by the same antibodies that recognize HBeAg (*32*).

Assembly has been studied extensively in vitro using a truncated form of HBV Cp, comprising the N-terminal assembly domain (amino acids 1−149) of strain *adyw* Cp expressed in *E. coli* (Cp149) (*38*). This protein lacks the C-terminal nucleic acid binding domain (amino acids 150−183), which is not required for assembly of empty capsids (*27*). In vitro assembly is a function of protein concentration, NaCl concentration, pH, and temperature (*6*, *38*). Assembly is nucleated by a trimer of Cp149 dimers, followed by rapid addition of subsequent dimers (*47*). HBV capsids are held together by a network of surprisingly weak intersubunit contacts (*6*), a property that may be a feature of many virus systems (*43*). However, capsids persist even under unfavorable conditions because kinetic effects (hysteresis) impede capsid dissociation (*34*).

An important hypothesis arising from in vitro assembly studies is that HBV Cp undergoes a conformational transition

[†] This work was supported by American Cancer Society Award RSG-99-339-04-MBC.

* To whom correspondence should be addressed. E-mail: adam-zlotnick@ouhsc.edu. Telephone: (405) 271-9030. Fax: (405) 271-3910.

[1] Abbreviations: Cp, core protein; Cp149, assembly domain of the core protein (amino acids 1−149); MALLS, multiangle laser light scattering; SEC, size-exclusion chromatograhy.

10.1021/bi049571k CCC: $27.50 © 2004 American Chemical Society
Published on Web 07/02/2004

concomitant with assembly (*6*). This change may correlate with differences in antigenicity (*32*). The effect of NaCl on Cp149 assembly is saturable (*6*), suggesting that specific binding of Na^+ or Cl^- may be instrumental in activating assembly. However, the NaCl concentrations used in vitro are far too great to be physiologically relevant, implying that another molecule is involved in regulating assembly in vivo. In this paper, we demonstrate that zinc and nickel (metals with similar tetrahedral coordination geometries) induce Cp149 assembly; products of assembly at micromolar zinc concentrations have capsid-like antigenicity. Other metal ions can induce assembly, but only at ionic strengths similar to those required for salt-mediated assembly. Zinc-induced assembly at 37 °C yields complete capsids. However, at very high zinc concentrations (or at 21 °C), assembly products are dominated by small oligomers, suggesting a kinetically trapped reaction. Computer simulations of assembly reactions suggest that this might arise from the loss of a kinetic distinction between nucleation and elongation phases of the assembly reaction; nucleation no longer limits the rate of assembly in zinc-mediated assembly reactions.

EXPERIMENTAL PROCEDURES

Protein Expression and Purification. Truncated HBV capsid protein (Cp149) dimers were expressed and purified from *E. coli* as described (*45*, *46*). Protein was quantitated by absorbance at 280 nm ($\epsilon = 60\,900\ M^{-1}\ cm^{-1}$ for Cp149). Cp149 was dialyzed from storage buffer into reaction buffer (50 mM HEPES pH 7.5, 2 mM DTT) before examination of zinc binding and capsid assembly.

Light Scattering. Assembly was monitored by 90° light scattering at 320 nm with a 3 nm band-pass in a SPEX Fluoromax-2 fluorometer (Jobin-Yvon SPEX, Edison, NJ) using a 0.3 cm path length cuvette (Hellma, Forest Hills, NY), as previously described (*47*); the intense scattered light was attenuated by a neutral density filter. Light scattering was either determined after a 24 h incubation under assembly conditions or monitored in real time during an assembly reaction. Assembly at 21 °C was initiated by mixing Cp149 in 50 mM HEPES pH 7.5 with buffered NaCl, $ZnCl_2$, $NiCl_2$, $MgCl_2$, $CaCl_2$, or KCl (all from Sigma, St Louis, MO) as appropriate. Zinc-mediated assembly reactions at 37 °C were performed as above except that Cp149 in 50 mM HEPES pH 7.5 was pre-equilibrated to 37 °C and then mixed with 37 °C-equilibrated unbuffered 2× salts comprising 0.3 M NaCl plus $ZnCl_2$.

Intrinsic Protein Fluorescence. Fluorescence spectra for HBV Cp149 were recorded at 21 or 37 °C over the range 300−400 nm with an excitation wavelength of 280 nm; all slits were set for a 1 nm band-pass. Typical reactions had 0.2 μM protein in the presence of 0−100 μM $ZnCl_2$ in 50 mM HEPES pH 7.5, either with or without 150 mM NaCl. Reactions were incubated for 20 min at 22 °C. To account for the increased emission and red shift observed in the fluorescence, titration data were converted to spectral center of mass (Vi (*33*)):

$$\mathrm{Vi} = \sum[\mathrm{F}^*\mathrm{wavenumber}]/\sum[\mathrm{F}] \qquad (1)$$

To determine the midpoint (mid) of the binding curve (an estimate of the average dissociation constant) and estimate the minimum number of zinc binding sites (*n*), data were fit to a single exponential curve, assuming ideal cooperativity between binding sites:

$$\mathrm{Vi} = \mathrm{Vi}_0 + (\mathrm{Vi}_\infty - \mathrm{Vi}_0)\left(1 - \frac{([\mathrm{Zn}]/\mathrm{mid})^n}{(1 + ([\mathrm{Zn}]/\mathrm{mid})^n)}\right) \qquad (2)$$

where Vi is the spectral center of mass observed at a specified [Zn], in the absence of zinc (Vi_0), or extrapolated to infinite zinc (Vi_∞). Values for Vi_∞, mid, and *n* were fit to data using KaleidaGraph (Synergy Software, Reading, PA).

Size Exclusion Chromatography (SEC) and Multiangle Laser Light Scattering (MALLS). Assembly reactions were examined by SEC on a Superose 6 10/30 column mounted on an ÄKTA FPLC with a UV detector (both from Amersham Biosciences, Piscataway, NJ) or on a Sephacryl S300 column mounted on a Shimadzu high performance liquid chromatography (HPLC) system equipped with an autosampler. For studies at 21 °C, the column was equilibrated with 50 mM HEPES pH 7.5, 50 mM NaCl, and $ZnCl_2$ as described. The same conditions were used for studies of 37 °C assembly reactions, except that the mobile phase was 25 mM HEPES pH 7.5, 150 mM NaCl.

SEC-MALLS was performed using a Superose 6 10/30 column, mounted either on a POROS Biosystems pump with an Optilab DSP refractometer (Wyatt Technology, Santa Barbara, CA) or on an ÄKTA FPLC with a UV detector. Light scattering was observed using a DAWN DSP 18-angle light-scattering detector (Wyatt Technology, Santa Barbara, CA). The column was pre-equilibrated with 50 mM HEPES pH 7.5 and 50 mM NaCl, with or without 50 μM $ZnCl_2$, as described in the appropriate figure legend. Zimm analysis of selected peaks was calculated by the program ASTRA, assuming a d*n*/d*c* refractive index increment of 0.185 for protein. Fractions were collected and analyzed by ELISA (see below).

ELISA Assays. Immulon 2 HB microtiter plates (Thermo Labsystems, Franklin, MA) were coated with protein samples overnight in 0.1 M sodium bicarbonate pH 9.5. Detection of capsid-specific antigen (HBcAg) was performed using monoclonal antibody MAB16988 (Chemicon, Temecula, CA) as primary antibody and horseradish peroxidase conjugated goat anti-murine IgG as secondary antibody (Sigma, St Louis, MO). After incubation with substrate (0.003% H_2O_2 and 1 mg/mL 1,2-phenylenediamine in 0.5 M NaCl buffered with 20 mM Na citrate pH 5.0), reactions were stopped by the addition of an equal volume of 2 M H_2SO_4. HBcAg was measured by absorbance at 490 nm. In our hands, MAB16988 is highly selective for assembled capsid (HBc) compared to unassembled dimer (HBeAg antigenicity), even though the primary sequences of the two antigens are the same; the signal attributable to dimer did not rise above the background at the antibody dilutions used.

Kinetic Simulations. Simulations of virus assembly kinetics were performed to demonstrate the basis of kinetic trapping. Calculations were performed using BERKELEY MADONNA (Berkeley Software, Berkeley, CA) for numerical integrations using a system of differential equations that describe polymerization of an icosahedron from 30 "dimeric" subunits, arranged to mimic HBV subunit geometry, as previously described (*11*). Briefly, in the complete capsid, each subunit is centered on an icosahedral twofold and makes four intersubunit contacts. Kinetic simulations were based

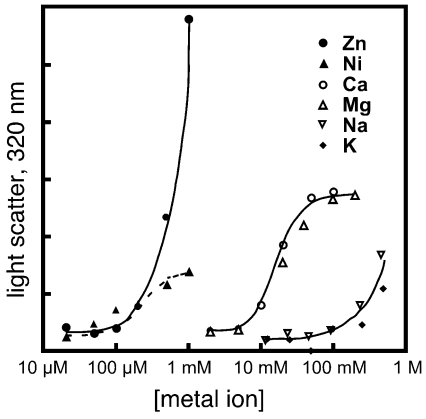

FIGURE 1: Induction of assembly by mono- and divalent cations. Assembly was monitored by 90° light scattering of assembly reactions containing 5 μM Cp149 in 50 mM HEPES pH 7.5 after a 24 h incubation at room temperature. For Na^+, K^+, Mg^{2+}, and Ca^{2+}, the ability to induce assembly correlates approximately with ionic strength. Zn^{2+} and Ni^{2+} induce assembly at concentrations at least 100-fold lower than those seen for the other divalent cations tested.

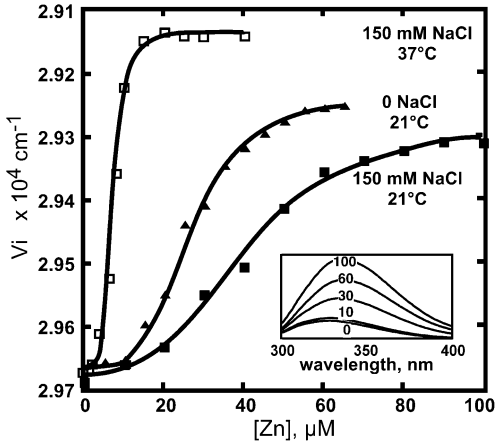

FIGURE 2: Intrinsic fluorescence of Cp149 increases with increasing Zn. Fluorescence emission spectra of 0.5 μM Cp149 were recorded in the presence of 0−100 μM zinc at 21 °C (inset, fluorescence corrected for fluorescence of buffer) or 37 °C (not shown). Spectra show zinc-dependent changes in intensity; the emission maximum shifts from 326 to 334 nm with increasing zinc concentration. Fluorescence was converted to spectral center of mass, Vi, to account for the shift in fluorescence maximum (eq 1). Sigmoidal titration curves suggest cooperative zinc binding (eq 2); see Table 1.

on the assumption that assembly occurs through a cascade of bimolecular reactions; that is, a single dimer is added to a partially assembled capsid at each step. The model also incorporates a nucleation step where a trimeric nucleus is formed; we have previously shown that the rate of HBV capsid formation is controlled by the rate of formation of a trimer of Cp149 dimers that initiates capsid formation (*47*). Required input values were the per-contact association constant ($K_{contact}$) and microscopic forward rate constants for nucleation (k_{nuc}) and elongation (k_{elong}). Rate constants for each back reaction were calculated from the association constant and the forward rate constants after adjustment for reaction degeneracy (*42*). For these calculations, the input values were [subunit] = 12 μM and $K_{contact} = 10^3$ M^{-1} (similar to experimental values for HBV (*6*)) and $k_{nuc} = 80$ M^{-1} s^{-1} and $k_{elong} = 80$ or 8000 M^{-1} s^{-1}, values that allow simulations with the 30 subunit model to match qualitatively the behavior of 120 subunit HBV.

RESULTS

Cp Assembly Is Induced by Metal Ions. Our previous studies of the thermodynamics of HBV capsid assembly showed that the magnitudes of enthalpy, entropy, and free energy saturably approach maximum values at high NaCl concentrations (*6*). We hypothesized that assembly was triggered by weak binding of salt to the capsid protein, inducing a conformational change. As the NaCl concentration required for assembly was significantly above physiological concentrations, we hypothesized that NaCl was inefficiently mimicking some in vivo activator of protein assembly.

Metal ions such as calcium, magnesium, and zinc are known to play important roles in both protein structure and function. We tested the ability of mono- and divalent cations to induce assembly of 5 μM capsid in 50 mM HEPES pH 7.5. All metal ions tested were in the form of chloride salts. When assembly was monitored by measuring light scattering after a 16 h incubation at 21 °C, it was found that assembly was induced by Na^+ and K^+ ions above 0.2 M (Figure 1), consistent with previous observations (*6*). Divalent cations Mg^{2+} and Ca^{2+} induced significant assembly at lower concentrations (50 mM); these concentrations correspond to slightly weaker ionic strengths than those required for assembly by monovalent cations. In contrast, we find that Zn^{2+} and Ni^{2+} induced assembly at much lower concentrations; increased light scattering was observed at ion concentrations of 200 μM and above. This suggested a specific and selective binding of Zn^{2+} ions; although it is not biologically relevant, Ni^{2+} has similar chemistry and tetrahedral geometry and can frequently be substituted for Zn^{2+} without losing biological activity. Because Zn^{2+} had the strongest effect, we decided to investigate further its possible role in Cp assembly.

Cp149 Binds Zn^{2+} Cooperatively. We used intrinsic protein fluorescence as a sensitive monitor for Zn^{2+} binding and changes in protein conformation. Assembly with NaCl caused intrinsic Cp149 fluorescence to increase by a factor of 2 with no shift in wavelength (*34*). When saturated with zinc (50 μM), the fluorescence intensity of 0.3 μM Cp149 increased approximately 6-fold, while the fluorescence emission maximum shifted from 326 to 334 nm (Figure 2). NaCl alone had no effect at similar concentrations (data not shown). These data showed binding and indicated that zinc affected Cp149 conformation.

Titration of 0.3 μM Cp149 with zinc led to a sigmoidal increase in intrinsic protein fluorescence, indicating cooperative binding of zinc (Figure 2). This protein concentration was too low to support capsid assembly, so any change observed would be due exclusively to a direct effect of zinc on the conformation of unassembled dimer. The midpoint of the binding curve was approximately 7 μM $ZnCl_2$ at 37 °C and between 25 and 50 μM at 21 °C, depending upon the NaCl concentration (Table 1). The midpoint provided an estimate of the dissociation constant. Fitting the data as described (methods) showed a power dependence on zinc concentration between 3 and 4.5 (Table 1), indicating that there are at least four zinc sites per dimer. Zinc binding was weaker at higher NaCl concentrations (midpoint value is

Table 1: Zinc Binding to Cp149 Examined by Intrinsic Fluorescence

	0 NaCl 21 °C	150 mM NaCl 21 °C	150 mM NaCl 37 °C
midpoint, μM	26.0 ± 0.7	41 ± 2	7.3 ± 0.1
sites/dimer	3.3 ± 0.3	3.0 ± 0.4	4.5 ± 0.3
R	0.9986	0.9970	0.9988

increased), probably due to weaker electrostatic interaction at higher ionic strength.

In contrast to the behavior of dimer, there was no detectable change in protein fluorescence when zinc was incubated with capsid (data not shown). Either there were no zinc binding sites in capsids, or binding zinc to Cp149 in capsid form did not induce further conformational change measurable by fluorescence. We note that the fluorescence of Cp149 in capsid form is already twice that of free Cp149, independent of ionic strength (*34*).

$ZnCl_2$ Enhances Kinetics of Capsid Assembly at 37 °C. Assembly reactions performed at 37 °C in 150 mM NaCl with $ZnCl_2$ showed that the rate of assembly (monitored by real-time light scattering) was significantly enhanced by as little as 5 μM $ZnCl_2$ (Figure 3A). The initial assembly rate increased with increasing zinc concentration to at least 50 μM $ZnCl_2$. The effect of zinc on assembly kinetics continued for total zinc concentrations well above those for which the change in fluorescence reached saturation (compare to Figure 2). This may be explained one of two ways: (i) the concentration of protein used in the assembly reactions (15 μM dimer) was much higher than that used in the fluorescence assay (0.3 μM), and thus, even at 50 μM $ZnCl_2$ the amount of Zn^{2+} present was below saturation (at least 4 Zn^{2+} per Cp149 dimer, see Table 1); (ii) only those binding events resulting in a change in intrinsic protein fluorescence were detectable in the binding assay; additional lower affinity binding events may have contributed to assembly without altering the fluorescence.

Size exclusion chromatography (Figure 3B) showed that the reaction at equilibrium (24 h at 37 °C) strongly resembled NaCl-induced assembly reactions; significant amounts of free subunit (dimer) and capsid were present, but assembly intermediates were undetectable. The yield of capsid from 15 μM Cp149 dimer at equilibrium was 10.7 ± 1.1 μM (as dimer equivalent, from 20 determinations) at 24 h, independent of zinc concentration. The extent of assembly was not significantly altered by the addition of zinc (Figure 3B). Examination of the products by EM and sucrose gradient centrifugation showed capsids which were morphologically normal (data not shown). This suggests that the role of zinc in assembly may be primarily to increase the rate of assembly but not the association constant: thus, the effect of zinc is kinetic. We have observed that a naturally occurring mutant of HBV, F97L, also enhances the kinetics of capsid assembly (P. Ceres et al., in press).

Cp149 Oligomers Accumulate in Zn-Induced Assembly at 21 °C. To further dissect the effect of zinc on assembly, we performed assembly reactions at 21 °C. Under these conditions, all phases of the assembly reaction were expected to be less rapid and changes were more readily detected. The products of $ZnCl_2$-mediated assembly were examined using SEC-MALLS. At 21 °C and 150 mM NaCl, in excess of 400 μM $ZnCl_2$ was required to induce assembly. When assembly reactions were conducted with 500 μM $ZnCl_2$, we observed that a heterogeneous pool of Cp149 oligomers accumulated (Figure 4). The major peak of oligomers ranged in molecular weight from 200 to 400 kDa, corresponding to 5−10 dimers. Over the course of several hours, the concentration of this pool increased at the expense of free dimer (data not shown). The concentration of capsid was small and increased very slowly. A similar SEC profile was observed for assembly reactions at 37 °C when the concentrations of $ZnCl_2$ (300 μM) and protein (16 μM) were very high (data not shown). Very high concentrations of zinc led to uncontrolled assembly in vitro, allowing the trapping of intermediates or aberrant products.

Zinc-Induced Assembly at 21 °C Yields Oligomers with Capsid-like Antigenicity. SEC-MALLS experiments of zinc assembly reactions run without zinc in the elution buffer shared many features with those described above: a small capsid peak, an oligomer peak corresponding to 5−10 dimers, and dimer (Figure 5). Even in the absence of $ZnCl_2$, the oligomer peak was sufficiently stable that it survived the

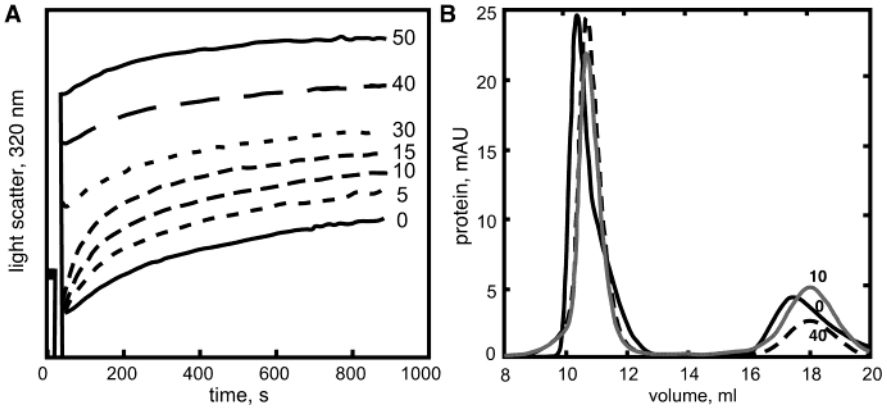

FIGURE 3: Zinc enhances the rate but not the extent of assembly of Cp149 at 37 °C. Capsid assembly was induced by NaCl, so reaction concentrations were 15 μM Cp149, 150 mM NaCl, and 0−50 μM $ZnCl_2$ as indicated. (A) Assembly kinetics were monitored by measuring increased light scattering at 320 nm over the first 15 min of the assembly reaction. (B) Selected examples of the effect of $ZnCl_2$ on assembly reactions at equilibrium. Assembly was allowed to proceed overnight, and then assembly products were examined by SEC using a Sephacryl S300 column (total volume approximately 27 mL, void volume approximately 9 mL) equilibrated in 25 mM HEPES, 150 mM NaCl. Capsid elutes at 10 mL, and dimer, at approximately 18 mL. The equilibrium concentrations of capsid and dimer were unaffected by the presence of zinc in the assembly reaction.

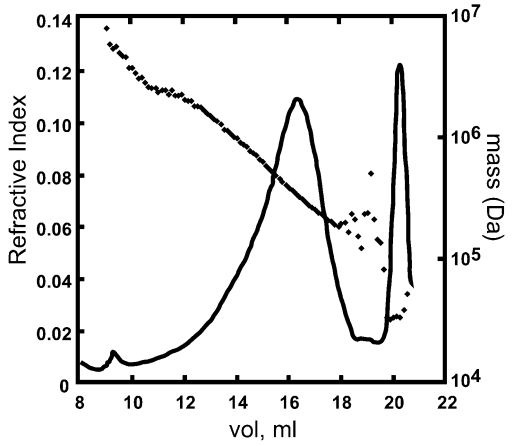

FIGURE 4: Zinc-mediated assembly reactions are kinetically trapped. Assembly reactions at 21 °C containing 15 μM Cp 149_2 and 500 μM $ZnCl_2$ in 50 mM HEPES pH 7.5 were analyzed at 6 h by SEC (solid line) on a Superose 6 column in 50 mM HEPES, 50 mM NaCl, 50 μM $ZnCl_2$, with molecular weights being determined by in-line MALLS (diamonds). Capsids elute at 8 mL, and dimer elutes at 20.5 mL under these conditions. Intermediates (eluting between 12 and 20 mL) are evident at least as early as 10 min after the initiation of assembly. Assembly reactions allowed to run overnight yielded aggregates (data not shown). The inclusion of $ZnCl_2$ in the elution buffer apparently stabilized some intermediate populations (compare to Figure 5B, run without zinc in the elution buffer). The molecular weight for the intermediates ranges from 200 to 400 kDa, corresponding to 5−10 dimers.

approximately 1 h required for elution. Additionally, we observed a peak eluting slightly faster than the dimer peak with the same apparent molecular weight as that of dimer. Fractions from three SEC-MALLS experiments were tested for capsid-specific antigenicity (Figure 5): (i) assembly induced by 500 μM $ZnCl_2$ at 21 °C (panel A), (ii) assembly induced by 50 μM $ZnCl_2$ and 150 mM NaCl at 37 °C (panel B), and (iii) control reactions without $ZnCl_2$ where assembly was induced by 300 mM NaCl at 21 °C (panel C). Conditions i and ii represent alternate outcomes for zinc-induced assembly. In the NaCl-induced reactions and zinc-induced assembly at 37 °C, only the capsid fractions were recognized in ELISAs using an HBc-specific monoclonal antibody. In the high $ZnCl_2$ reaction at 21 °C, the Cp149 oligomers were recognized, even though no complete capsid was present in these fractions. Note that all chromatographic separations were performed with at least 50 mM NaCl in the elution buffer to prevent protein from adsorbing to the column. Similar trapped assembly was observed at high $ZnCl_2$ concentrations at 37 °C (data not shown).

Chromatography of samples to be analyzed by ELISA was performed without zinc in the elution buffer to allow us to distinguish intermediates retaining HBc antigenicity from those which may have been generated after elution by prolonged incubation of protein with zinc. The presence of zinc in the elution buffer seemed to stabilize some intermediates that were not evident when zinc was left out of elution buffers: compare Figure 4 (eluted with zinc) to Figure 5 (no zinc in elution buffer). We chose to keep the zinc concentration in elution buffers low to prevent the formation of large aggregates which were sometimes observed after long incubations. Such aggregation could be reversed by the addition of EDTA to yield apparently normal dimers, indicating that the aggregates were not denatured protein.

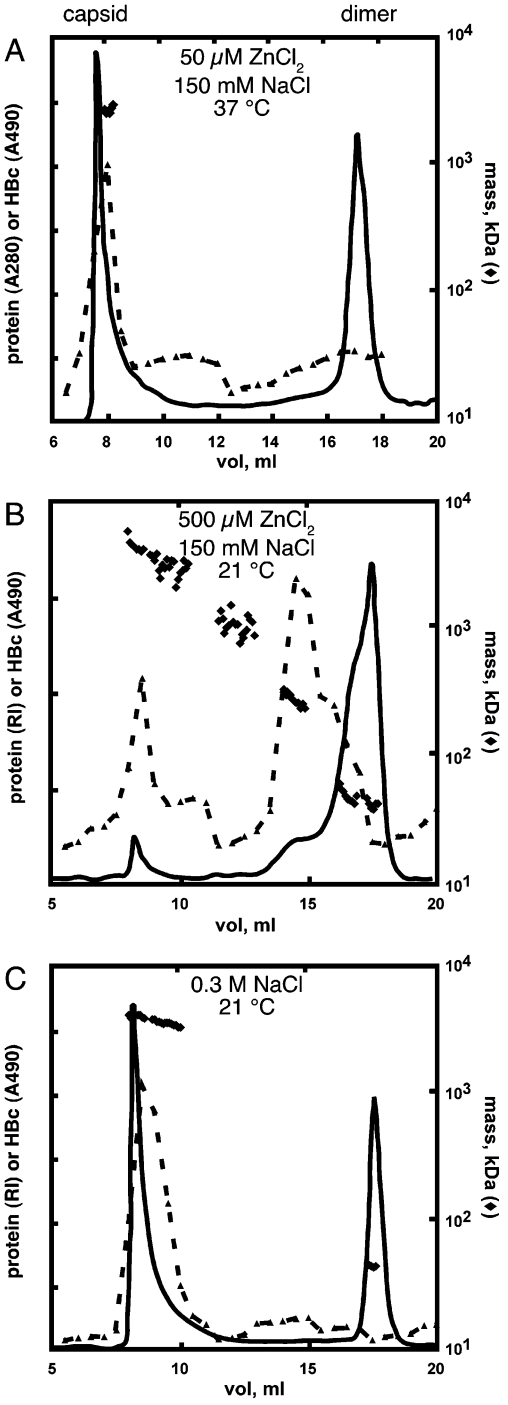

FIGURE 5: Assembly of wild-type Cp149 analyzed by SEC-MALLS and ELISA. Wild-type Cp149 (15 μM) was assembled with (A) 50 μM $ZnCl_2$ in 150 mM NaCl at 37 °C for 17 min, (B) 500 μM $ZnCl_2$ in 0.15 M NaCl at 21 °C for 2 h, or (C) 0.3 M NaCl at 21 °C overnight. Assembly reactions were resolved by SEC. Protein elution (solid line) was detected by absorbance at 280 nm (panel A) or refractive index (panels B and C). Molecular mass was determined from MALLS (diamonds). Fractions were assayed for capsid-specific antigenicity (HBc) by ELISA (triangles, dotted lines). Expected molecular weights for capsid (4 MDa) and dimer (35 kDa) were observed. Values for the protein signal (*y*-axis) were from 0.2 to 18.4 mAU at 280 nm for panel A, from 0.0020 to 0.1686 RIU (refractive index units) for panel B, and from 0.00 to 0.2690 RIU for panel C. ELISA horseradish peroxidase signals (also *y*-axis) were from 0.037 to 0.332 AU at 490 nm for panel A, from 0.040 to 0.304 for panel B, and from 0.041 to 1.04 A490U for panel C. Note that capsid eluted at approximately 8 mL and dimer eluted at 20.5 mL under these conditions, as for Figure 4.

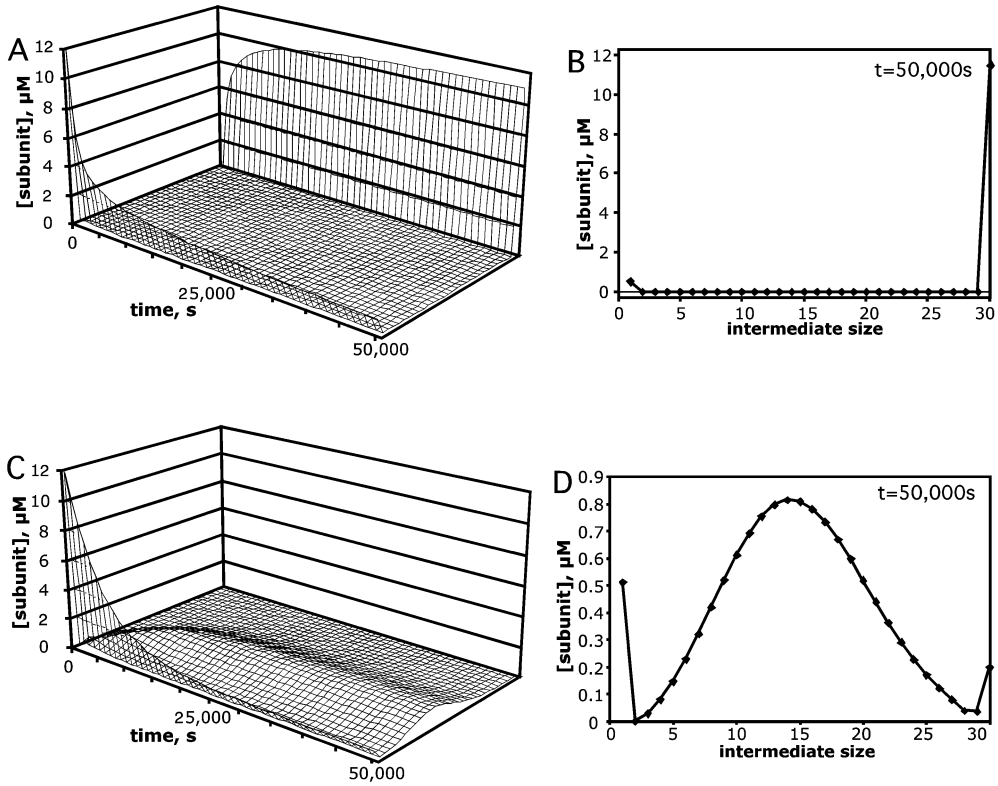

FIGURE 6: Simulations demonstrate kinetic trapping. For the kinetic simulations (A and C), the time courses of changes in the concentrations of free subunit (front wall), the different intermediates, and capsid (back wall) are shown. Panels B and D are "end on" views of panels A and C, showing profiles of the different species at 50 000 s. Each simulated reaction started with the same subunit concentration (12 μM) and per-contact association constant (10^3 M^{-1}). In a typical successful reaction (A and B), the elongation rate (k_{elong}, 8000 M^{-1} s^{-1}) is 100-fold faster than the nucleation rate (k_{nuc}, 80 M^{-1} s^{-1}); the reaction closely approaches equilibrium (*11*). These rate and association constants were chosen to put the simulations on the same scale as in vitro HBV assembly reactions. The "successful" simulation strongly resembled experimental data for assembly at 37 °C in the presence of low to moderate zinc concentrations (see Figure 3A). (B) Consistent with the experimental results (Figures 3B and 5A and B), the concentrations of intermediates at 50 000 s were very low. In a kinetically trapped reaction (C and D), though the equilibrium concentrations of all species are the same as those in the successful reactions, equilibrium was not achieved within 50 000 s. Trapping occurred because k_{nuc} and k_{elong} were set to the same value (80 M^{-1} s^{-1}); hence, there was no regulation of reaction initiation. (D) At 50 000 s the reaction mixture was dominated by metastable intermediates and a critical concentration of free subunit. The concentration of free subunit is the same in panels B and D. This profile resembled the distribution of intermediates observed when assembly was induced by high zinc concentrations (Figures 4 and 5C). In the simulation, the trapped reaction will eventually reach equilibrium, but very slowly (approximately 360 000 s, i.e., 4 days).

As the HBc antibody recognizes Cp149 in a conformation found in capsid but not in unassembled dimers, the finding that anti-HBc monoclonal antibodies recognized small protein oligomers (see Figure 3) indicated that the protein in the oligomers had been converted to the capsid-like conformation rather than simply being an aggregate of dimeric or denatured protein. The folded state was confirmed by the fact that circular dichroism (CD) spectra of protein assembled with zinc were essentially identical to spectra of both dimer and capsid (data not shown; see also refs *34* and *38*), demonstrating that the secondary structure of the protein did not change during zinc-mediated assembly.

Simulations of Assembly Show That Nucleation Rate Is Critical to Regulating Virus Assembly. To understand how zinc might influence the outcome of assembly reactions, we performed kinetic simulations of virus assembly where the relative rates of nucleation and elongation were manipulated. These simulations showed that intermediates accumulated when nucleation and elongation rates were similar, recapitulating experimental observations (Figure 6A,B). Kinetic simulations of capsid assembly were able to reproduce the behavior observed in zinc-induced assembly of Cp149. In simulations where the nucleation rate was much slower than the elongation rate, nucleation reactions were regulatory (*11*, *47*). Capsid and subunit were the dominant species present in successful assembly simulations (Figure 6A and B). These simulations resembled the NaCl assembly reactions of previous studies (*6*) and the successful zinc assembly reactions at 37 °C (Figure 3). When nucleation was not regulatory ($k_{nuc} = k_{elong}$), simulations produced a profile of intermediates (Figure 6C and D) that resembled the profile observed by SEC of Cp149 assembly induced by high $ZnCl_2$ concentrations (compare Figure 6 and Figures 4 and 5). The many partially assembled intermediates of the kinetic trap resulted in a critical concentration of free subunit (which is quantitatively similar to the $K_D$apparent observed in the assembly of closed spherical particles (*42*)).

DISCUSSION

Assembly of spherical viruses is likely to be a complex and highly regulated process involving interaction between capsid protein, genomic nucleic acid, and possibly other viral or host factors. For HBV, we proposed that a critical step is the generation of an assembly-active conformation for dimeric capsid subunits (*6*).

To better understand how assembly is controlled, we examined the ability of different salts to activate assembly. $ZnCl_2$ and $NiCl_2$, which both prefer tetrahedral coordination, induced assembly at micromolar concentrations, while other di- and monovalent cations tested could induce assembly only in the same range of ionic strength as seen for NaCl at 21 °C (Figure 1). We note that the millimolar concentrations of Ca^{2+} and Mg^{2+} seen to elicit assembly approach physiological ranges (*22*). Zinc-mediated oligomerization of Cp149 accompanied a change in intrinsic fluorescence and the acquisition of capsid-like antigenicity.

Studies of assembly at 37 °C and modest $ZnCl_2$ concentrations (2−50 μM) suggested that Zn^{2+} primarily affected the kinetics of assembly. To confirm this conclusion and to identify likely early intermediates in capsid assembly, we investigated trapped, $ZnCl_2$-induced assembly reactions (21 °C, high $ZnCl_2$). Our SEC and SEC-MALLS data showed that a significant amount of free dimer persisted in the presence of high zinc concentrations where small oligomers (5−10 dimers) accumulated. We have previously shown that, in successful HBV assembly reactions and analogous simulations, assembly was regulated by slow formation of nuclei comprised of a trimer of dimers (*47*). In these simulations, once nuclei were formed, they were rapidly consumed to form complete capsids; if too many nuclei were formed, the concentration of free subunit was too low to complete capsid formation at every nucleus (*47*). Kinetic trapping observed in simulations that mimicked assembly with high zinc was due to similar rates for nucleation and elongation. Trapped metastable (long-lived) intermediates accumulated in the presence of a critical concentration of free subunit, rather than being rapidly consumed as seen when nucleation is the rate-limiting step (Figure 6, compare panels B and D).

We have previously shown that nucleation is the rate-limiting step for capsid assembly (*44*, *47*). Assembly models suggest that, in general, the overall rate of assembly is much more sensitive to changes in the nucleation rate than the elongation rate (*11*). Results with simulations suggest that binding zinc preferentially affects nucleation of assembly. We have also observed assembly of the icosahedral plant virus cowpea chlorotic mottle virus (CCMV), where high concentrations of intermediates self-associate and inhibit the assembly of normal $T = 3$ capsids (*44*). Thus, the cause of kinetically trapped HBV assembly in the presence of high concentrations of zinc is probably not due to depletion of dimer but the availability of too many assembly-competent nuclei. This suggests that the rates of nucleation and elongation are differentially sensitive to changes in assembly conditions. Alternatively, the small oligomers observed in zinc-mediated assembly may be either aberrant nuclei or nonnative structures which cannot be elongated.

Our data indicate that zinc affects kinetics but not thermodynamics of assembly. We observe zinc induces a conformationally distinct form of Cp149 that we equate with an assembly-active state. Previous studies have shown that the rate-limiting step for capsid assembly is the formation of a nucleus, composed of a trimer of dimers (*47*). The assembly-active state is believed to be a precursor to this step and subsequent elongation (*6*). By this model (Figure 7), the rate of assembly in the presence of zinc is enhanced because the concentration of assembly-active dimer is increased. Based on the assumption of thermodynamic linkage (*39*, *40*), because zinc does not affect the thermodynamics of assembly, it should bind capsid as tightly as dimer. We were unable to directly measure binding of zinc to capsid, which suggests that zinc may bind very weakly to capsid and assembly-inactive dimer.

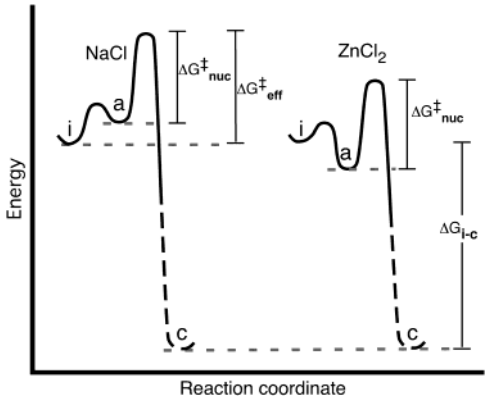

FIGURE 7: Proposed energy diagram of HBV capsid assembly. Assembly proceeds from inactive dimer (**i**) to an assembly-active form (**a**), which assembles into capsid (**c**). In NaCl-induced assembly, state **a** is energetically disfavored and thus relatively uncommon. The rate of assembly is limited in part by the concentration of **a**. Relative to **a**, the rate of nucleation is proportional to the activation energy, $\Delta G^{\ddagger}_{nuc}$. Relative to **i**, the effective activation energy, $\Delta G^{\ddagger}_{eff}$, is equal to $\Delta G^{\ddagger}_{nuc}$ plus the energy difference between **a** and **i** (ΔG_{a-i}). When present, Zn^{2+} stabilizes the assembly-active form, making **a** the favored species of dimer (and **i** relatively rare). Consequently, the nucleation rate in the presence of Zn^{2+} is proportional to $\Delta G^{\ddagger}_{nuc}$. The value for $\Delta G^{\ddagger}_{nuc}$ may or may not change in the presence of zinc. For clarity, the numerous intermediate oligomers between nucleus and capsid are represented by the thick dashed line.

The effect of zinc on HBV capsid assembly satisfies criteria for allostery (*21*, *26*): binding is cooperative and induces a change in fluorescence (Figure 2), indicating that binding is associated with conformational change; binding is associated with altered biological activity (capsid assembly) (*21*, *26*). At the mechanistic level, zinc binding may have several consequences for dimer structure: (i) zinc may bind to the assembly-inactive dimer and destabilize it, (ii) zinc may stabilize a capsid-like conformation of the dimer, or (iii) zinc binding may decrease the activation energy. Options ii and iii imply the existence of an intermediate state between capsid and dimer (Figure 7). This putative intermediate conformation is consistent with the distinct intrinsic fluorescence of Cp in the presence of zinc at low protein concentrations (Figure 2). Presumably, this intermediate is functionally analogous to the assembly-activated dimer we have previously proposed (*6*). Besides the changes in intrinsic fluorescence between dimer and capsid (*34*), the difference in recognition by anti-HBc antibodies demonstrates that there is at least a subtle change in the structure of the major HBc epitope located at the dimer interface (*7*, *31*). An active state or preassembly conformational change has also been observed in assembly of retroviruses (*17*).

Since no structural data are available for either the assembly-inactive dimer or any potential transitional forms, we examined the crystal structure (*41*) for the presence of potential zinc binding sites. Based on the results of the binding studies (Figure 2, Table 1), we expected at least four binding sites per dimer. We located one pair of putative symmetry-related zinc binding sites at the intrasubunit

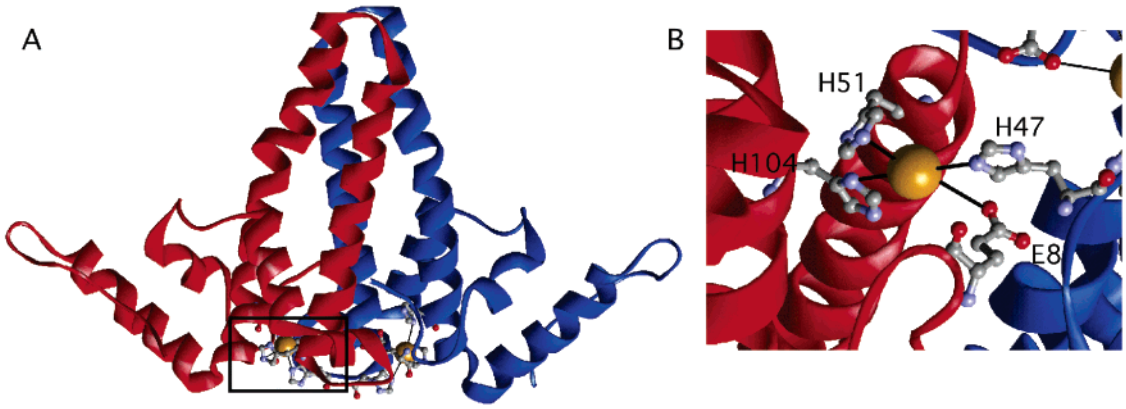

FIGURE 8: Putative symmetry-related Zn binding sites identified in a dimer, from the crystal structure of the HBV capsid (*41*). (A) Each site is comprised of E8, H51, and H104 from one half-dimer (red) and H47 from the other half-dimer (blue), viewed from the side, tangent to the capsid surface. (B) The same site shown boxed in part A enlarged and viewed from inside the capsid.

interface (Figure 8). These sites are composed of E8, H51, and H104 from one half-dimer and H47 from another. We note this complement of ligands is not exclusive to binding zinc (*1*). Comparison of the sequences of hepadnavirus core (capsid) proteins shows that H47, H51, and H104 are conserved throughout avian and mammalian capsid proteins (*5*). E8 is conserved in mammalian hepadnaviruses but is replaced by its functional analogue aspartate in avian viruses. In contrast, of the four cysteine residues in the protein (C48, C61, C107, and C183), only C107 is conserved across mammalian and avian species, and all are dispensable for assembly of capsid (*27*). Viruses where H47 and H51 were mutated to leucine were not replication competent (*10*). Histidine at position 52 is not conserved between mammalian and avian hepadnavirus core proteins (*5*) and can be mutated to leucine without significantly affecting total protein levels (*10*). Thus, the residues we propose as zinc ligands are evolutionarily highly conserved and may affect Cp stability.

Zinc atoms may be readily docked into the putative zinc sites with some rearrangement of the side chain torsional angles, but without movement of the main chains. The distance from the modeled zinc atom to the ligating groups averaged 2.6 ± 0.6 Å, only slightly longer than typically observed in crystal structures of zinc-binding enzymes with bound zinc (*18*). A better fit could be accomplished and more sites identified; however, we cannot justify more extensive modeling studies in the absence of more structural information, such as structures of assembly-active and -inactive dimer. Each putative zinc site involves residues from both halves of the dimer, suggesting that zinc binding could change the spatial relationship of the two half-dimers, resulting in an allosteric effect; thus, zinc binding at one site would influence the geometry and binding affinity at the symmetry-related site. The biological implications of allostery in virus assembly are significant: an allosteric activator would allow tight regulation of assembly.

The exact biological role of metal ions in HBV capsid assembly is still unclear. We have shown that, at physiologically relevant temperature and ionic strength, micromolar zinc concentrations can induce a change in HBV Cp conformation and enhance the rate of capsid assembly in vitro. Based on the comparison of the behavior of zinc-mediated assembly reactions with model simulations, the alteration in dimer conformation seems to specifically affect nucleation. The role of zinc in protein structure is well documented (*3*, *12*, *18*). Recent studies have demonstrated that zinc atoms may act as weakly bound linkers between proteins involved in intracellular signaling (*20*), although zinc atoms are generally tightly bound by proteins. The intracellular concentration of free zinc is tightly regulated (*28*, *29*). It has been proposed that zinc is generally transferred directly from a donor to an acceptor molecule (*16*). Also, free zinc ions may not be the true in vivo initiator but may merely mimic interactions with other molecule(s) within the infected cell. Thus, the actual activator could be a zinc atom donated by or shared with another protein, which may allow the virus to recruit other viral or cellular proteins to the assembly virion. We have identified a putative zinc binding site, but we note that the set of ligands we describe is not exclusive to binding of zinc (*1*). Thus, zinc in vitro may be acting as a molecular mimic of another metal ion or some other molecule.

The understanding that activation of capsid protein for assembly involves a structural transition opens the possibility of a novel target for antiviral drugs that would either inhibit activation or increase it, leading to the formation of aberrant and presumably noninfectious particles in vivo. Examples of such potential drugs targeting HBV have already been described. BisANS preferentially binds dimeric Cp to inhibit and/or misdirect assembly in vitro (*45*). Heteroaryldihydropyrimidines (HAPs) inhibit accumulation of cores and lead to Cp degradation by proteasomes (*10*, *14*, *37*). The alkylated imino sugar *n*-(*n*-nonyl)deoxygalactonojirimycin (n,nDGJ) also seems to affect accumulation of core particles without interfering with Cp transcription or translation (*23*, *24*). Further understanding of how HBV Cp is activated for assembly will not only contribute to design of better drugs for the treatment and prevention of HBV, but may also lead to a more generalized understanding of the regulation of assembly of other viruses.

ACKNOWLEDGMENT

We thank the Oklahoma Medical Research Foundation Imaging Facility for use of its electron microscope, and we thank Bruce Baggenstoss for assistance with SEC-MALLS. We thank Jennifer Johnson and Christina Bourne for helpful discussions and critical reading of this manuscript.

NOTE ADDED AFTER ASAP POSTING

This paper was inadvertently posted on the Web on 07/02/04. The correct version was posted 07/02/04.

REFERENCES

1. Banerjee, S., Wei, B., Bhattacharyya-Pakrasi, M., Pakrasi, H., and Smith, T. (2003) Structural determinants of metal specificity in the zinc transport protein ZnuA from *Synechocystis* 6803. *J. Mol. Biol. 333*, 1061−1069.
2. Belnap, D., Watts, N., Conway, J., Cheng, N., Stahl, S., Wingfield, P., and Steven, A. (2003) Diversity of core antigen epitopes of hepatitis B virus. *Proc. Natl. Acad. Sci. U.S.A. 100*, 10884−10889.
3. Berg, J. M., and Godwin, H. A. (1997) Lessons from zinc-binding peptides. *Annu. Rev. Biophys. Biomol. Struct. 26*, 357−71.
4. Bottcher, B., Wynne, S. A., and Crowther, R. A. (1997) Determination of the fold of the core protein of hepatitis B virus by electron cryomicroscopy. *Nature 386*, 88−91.
5. Bringas, R. (1997) Folding and assembly of hepatitis B virus core protein: A new model proposal. *J. Struct. Biol. 118*, 189−196.
6. Ceres, P., and Zlotnick, A. (2002) Weak protein−protein interactions are sufficient to drive assembly of hepatitis B virus capsids. *Biochemistry 41*, 11525−11531.
7. Conway, J. F., Cheng, N., Zlotnick, A., Stahl, S. J., Wingfield, P. T., Belnap, D. M., Kanngiesser, U., Noah, M., and Steven, A. C. (1998) Hepatitis B virus capsid: localization of the putative immunodominant loop (residues 78 to 83) on the capsid surface, and implications for the distinction between c and e-antigens. *J. Mol. Biol. 279*, 1111−21.
8. Conway, J. F., Cheng, N., Zlotnick, A., Wingfield, P. T., Stahl, S. J., and Steven, A. C. (1997) Visualization of a 4-helix bundle in the hepatitis B virus capsid by cryo-electron microscopy. *Nature 386*, 91−94.
9. Crowther, R. A., Kiselev, N. A., Bottcher, B., Berriman, J. A., Borisova, G. P., Ose, V., and Pumpens, P. (1994) Three-dimensional structure of hepatitis B virus core particles determined by electron cryomicroscopy. *Cell 77*, 943−950.
10. Deres, K., Schröder, C., Paessens, A., Goldmann, S., Hacker, H., Weber, O., Krämer, T., Niewöhner, U., Pleiss, U., Stoltefuss, J., Graef, E., Koletzki, D., Masantschek, R., Reimann, A., Jaeger, R., Gro*β*, R., Beckermann, B., Schlemmer, K.-H., Haebich, D., and Rübsamen-Waigmann, H. (2003) Inhibition of hepatitis B virus replication by drug induced depletion of nucleocapsids. *Science 299*, 893−896.
11. Endres, D., and Zlotnick, A. (2002) Model-based analysis of assembly kinetics for virus capsids or other spherical polymers. *Biophys. J. 83*, 1217−1230.
12. Frankel, A. D., Berg, J. M., and Pabo, C. O. (1987) Metal-dependent folding of a single zinc finger from transcription factor IIIA. *Proc. Natl. Acad. Sci. U.S.A. 84*, 4841−5.
13. Ganem, D. (1996) in *Fields Virology* (Fields, B. N., Knipe, D. M., Howley, P. M., Chanock, R. M., Melnick, J. L., Monath, T. P., Roizman, B., and Straus, S. E., Eds.) pp 2703−2737, Lippincott−Raven Publishers, Philadelphia, PA.
14. Hacker, H., Deres, K., Mildenberger, M., and Schroder, C. (2003) Antivirals interacting with hepatitis B virus core protein and core mutations may misdirect capsid assembly in a similar fashion. *Biochem. Pharmacol. 66*, 2273−2279.
15. Hollinger, F. B. (1996) in *Fields Virology* (Fields, B. N., Knipe, D. M., Howley, P. M., Chanock, R. M., Melnick, J. L., Monath, T. P., Roizman, B., and Straus, S. E., Eds.) pp 2738−2808, Lippincott−Raven Publishers, Philadelphia, PA.
16. Jacob, C., Maret, W., and Vallee, B. (1998) Control of zinc transfer between thionein, metallothionein, and zinc proteins. *Proc. Natl. Acad. Sci. U.S.A. 95*, 3489−3494.
17. Johnson, M., Scobie, H., Ma, Y., and Vogt, V. (2002) Nucelic acid-independent retrovirus assembly can be driven by dimerization. *J. Virol. 76*, 11177−11185.
18. Karlin, S., and Zhu, Z.-Y. (1997) Classification of mononuclear zinc metal sites in protein structures. *Proc. Natl. Acad. Sci. U.S.A. 94*, 14231−14236.
19. Kenney, J. M., von Bonsdorff, C. H., Nassal, M., and Fuller, S. D. (1995) Evolutionary conservation in the hepatitis B virus core structure: comparison of human and duck cores. *Structure 3*, 1009−1019.
20. Kim, P., Sun, Z.-Y., Blacklow, S., Wagner, G., and Eck, M. (2003) A zinc clasp structure tethers Lck to T cell coreceptors CD4 and CD8. *Science 301*, 1725−1728.
21. Koshland, D. E. J., Némethy, G., and Filmer, D. (1966) Comparison of experimental binding data and theoretical models in proteins containing subunits. *Biochemistry 5*, 365−385.
22. Krupp, M. (1992) *Normal laboratory values*, Lange Medical Publications, Los Altos, CA.
23. Lu, X., Tran, T., Simsek, E., and Block, T. (2003) The alkylated imino sugar, *n*-(*n*-nonyl)-deoxygalactonojirimycin, reduces the amount of hepatitis B virus nucleocapsid in tissue culture. *J. Virol. 77*, 11933−11940.
24. Mehta, A., Conyers, B., Tyrrell, D., Walters, K.-A., Tipples, G., Dwek, R., and Block, T. (2002) Structure−activity relationship of a new class of anti-hepatitis B virus agents. *Antimicrob. Agents Chemother. 46*, 4004−4008.
25. Milich, D. R., McLachlan, A., Stahl, S., Wingfield, P., Thornton, G. B., Hughes, J. L., and Jones, J. E. (1988) Comparative immunogenicity of hepatitis B virus core and e antigens. *J. Immunol. 141*, 3617−3624.
26. Monod, J., Wyman, J., and Changeaux, J.-P. (1965) On the nature of allosteric transitions: a plausible model. *J. Mol. Biol. 12*, 88−118.
27. Nassal, M. (1992) Conserved cysteines of the hepatitis B virus core protein are not required for assembly of replication-competent core particles nor for their envelopment. *Virology 190*, 499−505.
28. Outten, C. E., and O'Halloran, T. V. (2001) Femtomolar sensitivity of metalloregulatory proteins controlling zinc homeostasis. *Science 292*, 2488−92.
29. Peck, E., Jr., and Ray, W., Jr. (1971) Metal complexes of phosphoglucomutase in vivo. *J. Biol. Chem. 246*, 1160−1167.
30. Salfeld, J., Pfaff, E., Noah, M., and Schaller, H. (1989) Antigenic determinants and functional domains in core antigen and e antigen from hepatitis B virus. *J. Virol. 63*, 798−808.
31. Sällberg, M., Rudén, U., Magnius, L., Harthus, H., Noah, M., and Wahren, B. (1991) Characterisation of a linear binding site for a monoclonal antibody to hepatitis B core antigen. *J. Med. Virol. 33*, 248−252.
32. Seifer, M., Zhou, S., and Standring, D. N. (1993) A micromolar pool of antigenically distinct precursors is required to initiate cooperative assembly of hepatitis B virus capsids in Xenopus oocytes. *J. Virol. 67*, 249−257.
33. Silva, J. L., and Weber, G. (1988) Pressure-induced dissociation of brome mosaic virus. *J. Mol. Biol. 199*, 149−59.
34. Singh, S., and Zlotnick, A. (2003) Observed hysteresis of virus capsid disassembly is implicit in fundamental kinetic models of association and dissociation. *J. Biol. Chem. 278*, 18249−18255.
35. Stannard, L. M., and Hodgkiss, M. (1979) Morphological irregularities in Dane particle cores. *J. Gen. Virol. 45*, 509−514.
36. Summers, J., and Mason, W. S. (1982) Replication of the genome of a hepatitis B-like virus by reverse transcription of an RNA intermediate. *Cell 29*, 403−415.
37. Weber, O., Schlemmer, K.-H., Hartmann, E., Hagelshuer, I., Paessens, A., Graef, E., Deres, K., Goldmann, S., Niewohner, U., Stoltefuss, J., Haebich, D., Ruebsamen-Waigmann, H., and Wohlfiel, S. (2002) Inhibition of human hepatitis B (HBV) by a novel nonnucleosidic compound in a transgenic mouse model. *Antiviral Res. 54*, 69−78.
38. Wingfield, P. T., Stahl, S. J., Williams, R. W., and Steven, A. C. (1995) Hepatitis core antigen produced in Escherichia coli: subunit composition, conformational analysis, and in vitro capsid assembly. *Biochemistry 34*, 4919−4932.
39. Wyman, J. (1984) Linkage graphs: a study in the thermodynamics of macromolecules. *Q. Rev. Biophys. 17*, 453−488.
40. Wyman, J., and Gill, S. (1990) *Binding and Linkage: Functional Chemistry of Biological Macromolecules*, University Science Books, Herndon, VA.
41. Wynne, S. A., Crowther, R. A., and Leslie, A. G. W. (1999) The Crystal Structure of the Human Hepatitis B Virus Capsid. *Mol. Cell 3*, 771−780.
42. Zlotnick, A. (1994) To build a virus capsid. An equilibrium model of the self-assembly of polyhedral protein complexes. *J. Mol. Biol. 241*, 59−67.
43. Zlotnick, A. (2003) Are weak protein−protein interactions the general rule in capsid assembly? *Virology 315*, 269−274.
44. Zlotnick, A., Aldrich, R., Johnson, J. M., Ceres, P., and Young, M. J. (2000) Mechanism of Capsid Assembly for an Icosahedral Plant Virus. *Virology 277*, 450−456.

45. Zlotnick, A., Ceres, P., Singh, S., and Johnson, J. M. (2002) A small molecule inhibits and misdirects assembly of hepatitis B virus capsids. *J. Virol. 76*, 4848−4854.
46. Zlotnick, A., Cheng, N., Conway, J. F., Booy, F. P., Steven, A. C., Stahl, S. J., and Wingfield, P. T. (1996) Dimorphism of hepatitis B virus capsids is strongly influenced by the C-terminus of the capsid protein. *Biochemistry 35*, 7412−7421.
47. Zlotnick, A., Johnson, J. M., Wingfield, P. W., Stahl, S. J., and Endres, D. (1999) A theoretical model successfully identifies features of hepatitis B virus capsid assembly. *Biochemistry 38*, 14644−14652.

BI049571K